



# Sound Propagation in Lined Annular Ducts with Mean Swirling Flow

A.L.P. Maldonado \*

R.J.Astley †

J.Coupland ‡

G.Gabard §

*Institute of Sound and Vibration Research, University of Southampton, Southampton, SO17 1BJ, UK*

D. Sutliff ¶

*NASA Glenn Research Center, Acoustics Branch, Cleveland, OH, 44135.*

The current trends for turbofan engines are towards shorter nacelles and increased distances between the fan and the outlet guide vanes. This leads to an overall reduction in lined surface areas as well as an increase in the relative importance of the interstage liner, which is the liner placed between the rotor blades and the stator vanes. So far most of the efforts have been on liners for intakes and bypass ducts (in terms of physical insight, prediction methods and experimental data). The interstage is different in that the liner is subject to a mean flow with a strong swirl component and shear.

This paper aims to evaluate the effect of swirl on liner attenuation in annular ducts. The analysis presented is based on the governing equations for an isentropic swirling mean flow and a homentropic unsteady field. The eigenvalue problem is obtained by applying normal mode analysis to the linearized Euler Equations together with the Ingard-Myers boundary condition. Mean flow properties are assumed to vary with radius only. A fourth order finite difference code is compared against published results for specific flows such as solid body and free vortex swirl. Results from the Finite Difference Code are compared to measured data from the Advanced Noise Control Fan (ANCF) from NASA Glenn Research Center.

---

\*PhD Student, analuisamaldonado@gmail.com, AIAA Member.

†Professor, rja@isvr.soton.ac.uk, AIAA Member.

‡Visiting Research Associate, J.Coupland@soton.ac.uk, AIAA Member

§Associate Professor, g.gabard@soton.ac.uk, AIAA Member

¶Aerospace Engineer, daniel.l.sutliff@nasa.gov, AIAA Member

## I. Introduction

The swirling mean flow between the rotor and the stator is a key aspect when modelling turbomachinery noise in the interstage region where the swirl is of the order of 15 to 45 percent of the mean axial velocity<sup>5, 10</sup>. Swirl can prevent unsteady disturbances from reaching the walls and make expensive wall treatments ineffective.<sup>19</sup> The swirl changes the phase speed relative to the mean flow.<sup>19</sup> If on the one hand the relative phase speed decreases in modes that rotate in the same direction as the swirl and those modes become more cut-off, on the other hand, the relative phase speed increases in modes that rotate in the opposite direction as the swirl and they become more cut-on as the swirl increases<sup>1, 2</sup>. The downside is that modelling of ducted swirling flows is more challenging than parallel flows, since compressible and rotational phenomena are coupled.<sup>2</sup> One has to solve the 3D linearized Euler equations instead of a single convected wave equation.<sup>10</sup>

In the last 30 years, several researchers have studied the behaviour of swirling flows with different properties and classified the modes into families with similar characteristics.<sup>1, 15, 19, 20</sup> For uniform flows, unsteady disturbances are classified as vortical and entropical waves, that are purely convected by the flow, and acoustic waves. In hard-walled ducts, acoustic waves propagate unattenuated or decay exponentially.<sup>17</sup> Modes propagating in swirling flows are classified into acoustic modes, nearly convected modes and continuous spectrum. The well-known acoustic modes are directly related to the compressibility of the fluid. Pressure-dominated, they carry most of the unsteady pressure of the flow and are composed of cut-on and cut-off modes.<sup>23</sup> The nearly convected modes,<sup>14</sup> are related to the swirl of the mean flow. They are discrete hydrodynamic modes that carry a slight pressure component and convect at a speed similar (although not exactly) to the mean flow speed. The continuum spectrum is a set of the purely convected modes, which are a continuum of modes whose existence was reported by Kerrebrock<sup>14, 13</sup>. The derivative of these modes is such that the convective derivative  $D/Dt$  is zero.

Studies of propagation of small disturbances in a duct with mean swirling flow dates back to 1977. By using normal mode analysis, Kerrebrock<sup>14</sup> showed that vorticity, entropy and pressure modes were coupled in the presence of swirl. He pointed out that the shear disturbances are not purely convected by the mean flow, but rather they also carry a slight pressure component with them and are termed nearly-convected modes. Solid body rotation, free vortex swirl, constant swirl profiles or a superposition of them have been analysed over the last years. Important works in the field were performed by Kerrebrock<sup>13, 14</sup>, Kousen<sup>15, 16, 17</sup>, Golubev & Atassi<sup>5, 6</sup>, Tam & Ariault<sup>22</sup>, Nijboer<sup>18</sup>, Guan et al<sup>10, 9</sup>, Cooper & Peake<sup>2, 1</sup>, Cooper<sup>3</sup>, Posson & Peake<sup>20</sup> and Heaton & Peake<sup>11</sup>.

The most common methods used to obtain solutions for the Linearized Euler Equations are initial value analysis and normal mode analysis. Concerned with the fact that in swirling compressible ducted flows the question of completeness cannot be easily ascertained, Tam & Ariault<sup>22</sup> proposed an initial value analysis to make the complete rigorous analysis of the wave modes and seek clarification to the families of modes generated by hard-wall inviscid swirling compressible ducted flows. Kousen<sup>15, 16, 17</sup>, Golubev & Atassi<sup>5, 6</sup>, Guan et al<sup>10, 9</sup> performed a normal mode analysis instead. Based on the method of separation of variables, the normal mode analysis is the method used in this paper. The only difference is that Golubev & Atassi decomposed the disturbance velocity into a vortical and a potential part.

Isentropic mean flow were investigated by Kousen<sup>15, 16, 17</sup>, Guan & Wang<sup>9</sup> and Golubev & Atassi<sup>4, 5, 6</sup>, while non-isentropic mean flow with constant mean density was analysed by Tam & Ariault<sup>22</sup> and Guan & Wang.<sup>10</sup> Tam & Ariault<sup>22</sup> consider constant density mean flow, while this assumption is not made by Guan & Wang.<sup>10</sup> Nijboer<sup>18</sup> analysed the testcases proposed by Tam & Ariault<sup>22</sup> and Kousen<sup>16</sup> pointing out that the authors are comparing slightly different mean flows and that this leads to different results in some cases. Differences between results from those cases are negligible if the mean swirl Mach number is small ( $M_{\phi_0} \sim 0.1$ ). By comparing results for isentropic flow and results for constant density flow the author concludes that although the eigenvalues show the same patterns, the mean density variation affects the stability of the modes of the swirling flow. Heaton & Peake,<sup>11</sup> highlighted that the uniform density causes the appearance of an unstable mode found by Tam & Ariault<sup>22</sup> and that in reality it is expected that the density increases with radius in a compressible swirling flow because of increase in pressure to balance the centrifugal forces.

The effect of non-uniform mean entropy on eigenmodes was analysed by Guan & Wang<sup>9</sup> for a hard-walled straight annular duct with swirling flow and by Cooper<sup>3</sup> for a slowly varying duct with mean swirling flow. It is shown that modes become more cut-on in the presence of positive entropy gradients and less propagating in the presence of negative entropy gradients when compared to uniform entropy regimes. The higher the swirl, the higher the entropy is.

Published results for sound propagation in lined swirling flows are limited. Guan et al<sup>9</sup> used a Chebyshev polynomial spectral method to calculate the eigenvalues of the three-dimensional Linearized Euler Equations and used two different mode-matching schemes to calculate the sound transmission in ducts. They compared the two mode-

matching methods between themselves and with a finite element method and compared the results between themselves. A spectral collocation technique was used in which the solution is assumed to be composed of a linear combination of basic functions. The function is discretized in the physical space at some chosen points, called collocation points and the solution is forced to satisfy the partial differential equations only at the collocation points. A normal mode analysis is performed and the modified mode matching scheme proposed by the authors is used to evaluate the effect of the swirling flow on the sound power transmission loss and to conduct liner optimization in the impedance plane. Posson & Peake<sup>20</sup> derive an acoustic analogy that accounts for swirling flow and liners. They carry out a parametric analysis and apply the methodology to study the effect of swirlin mean flow on fan trailing edge broadband noise.

In this paper the effect of swirl on liner attenuation is evaluated. The governing equations are derived for an isentropic swirling mean flow and a homentropic unsteady field. The eigenvalue problem is obtained by applying the normal mode analysis to the linearized Euler Equations together with the Ingard-Myers Boundary Condition.<sup>12</sup> Properties are assumed to vary at most with radius. A fourth order finite difference code is compared to published results of specific flows such as solid body and free vortex swirl. The method is then applied to more realistic interstage flow profiles and liners.

## II. Duct Mode Propagation Theoretical Model

### II.A. Governing Equations

The governing equations for an isentropic perfect gas are the conservation of mass, conservation of momentum and energy equation together with the constitutive equation of state.

$$\frac{\partial \rho}{\partial t} + \nabla \cdot (\rho \mathbf{u}) = 0, \quad (1)$$

$$\rho \frac{D\mathbf{u}}{Dt} + \nabla p = 0, \quad (2)$$

$$\frac{Ds}{Dt} = 0, \quad (3)$$

$$\rho_0 c_0^2 = \gamma p_0, \quad (4)$$

or, if combined with the continuity equation and with the constitutive equation of state, the energy equation can be written in terms of pressure as:

$$\frac{Dp}{Dt} + \gamma p \nabla \cdot \mathbf{u} = 0, \quad (5)$$

where  $\rho$  is the density,  $t$  is the time component,  $\mathbf{u}$  is the velocity vector,  $p$  is the pressure and  $D/Dt$  is the material derivative operator, given by:

$$\frac{D}{Dt} = \frac{\partial}{\partial t} + \mathbf{u} \cdot \nabla \quad (6)$$

If each variable is decomposed into a steady mean value, represented by the subscript zero, and a fluctuating value, represented by the superscript dash

$$p = p_0 + p^{'}, \quad \rho = \rho_0 + \rho^{'}, \quad \mathbf{u} = \mathbf{u}_0 + \mathbf{u}^{'}, \quad (7)$$

and substituted in Equations (1) to (6), two sets of equations are obtained. The first set of equations governs the mean flow, while the other set governs the perturbation field.

### II.B. Mean Flow

The steady Euler equations for the mean field for an isentropic perfect gas are given by:<sup>2</sup>

$$\nabla \cdot (\rho_0 \mathbf{u}_0) = 0 \quad (8)$$

$$\rho_0 \mathbf{u}_0 \cdot \nabla \mathbf{u}_0 + \nabla p_0 = 0 \quad (9)$$

$$\mathbf{u}_0 \cdot \nabla p_0 + \gamma p_0 \nabla \cdot \mathbf{u}_0 = 0 \quad (10)$$

Assume a duct with constant inner and outer radius. The mean flow is steady, axisymmetric and has zero radial velocity. Its axial and azimuthal velocities are only dependent upon the radius,<sup>19</sup>

$$\mathbf{u}_0 = u_\phi(r)\mathbf{e}_\phi + u_{0x}(r)\mathbf{e}_x. \quad (11)$$

In interstage regions of turbofan engines, the fan generates a strong swirling flow and the azimuthal velocity cannot be neglected.<sup>10</sup> When swirl is included, mean variables such as pressure, density and speed of sound are not uniform any more. Substituting (11) in the steady Euler equations, the continuity equation is satisfied and the pressure gradient is obtained from the momentum equation for the radial, azimuthal and axial directions.<sup>15</sup>

$$\frac{\partial p_0}{\partial r} = \rho_0 \left( \frac{u_{0\phi}^2}{r} \right), \quad \frac{\partial p_0}{\partial \phi} = 0, \quad \frac{\partial p_0}{\partial x} = 0. \quad (12)$$

Since entropy is assumed to be constant along the flow, the product  $p_0 \rho_0^{-\gamma}$  is constant and the density gradient is given by:

$$\frac{\partial \rho_0}{\partial r} = \frac{\rho_0}{\gamma p_0} \frac{\partial p_0}{\partial r} \quad (13)$$

The speed of sound, for instance, is obtained from the equation for a perfect gas:

$$c_0^2 = \frac{\gamma p_0}{\rho_0} \quad (14)$$

Differentiating Equation (14) in relation to the radius, substituting (12) and (13) and integrating between the inner and outer radius:

$$c_0^2(r) = c_0^2(r_{out}) - (\gamma - 1) \int_r^{r_{out}} \frac{u_{0\phi}^2}{r} dr \quad (15)$$

The mean variables are non-dimensionalized by the respective values at the outer radius as follows:

$$c_0^* = c_0 / c_{0out} \quad (16)$$

$$\rho_0^* = \rho_0 / \rho_{0out} \quad (17)$$

$$p_0^* = \frac{p_0}{c_{0out}^2 \rho_{0out}}, \quad (18)$$

where  $\rho_{0out}$  and  $c_{0out}$  are the reference values of mean density and the mean sound speed at the outer radius. If the isentropic relations are applied between two radial locations, say, a point inside the duct and the outer wall, the following relations are obtained:

$$p^* = (\rho^*)^\gamma \quad (19)$$

$$(c_0^*)^2 = \frac{p^*}{\rho^*} \quad (20)$$

and mean flow variables as a function of radius for an isentropic flow are given in the non-dimensional form by:

$$c_0^{*2}(r^*) = 1 - (\gamma - 1) \int_{r^*}^1 \frac{u_{0\phi}^{*2}}{r^*} dr^*, \quad (21)$$

$$\rho_0^*(r^*) = (c_0^{*2})^{\frac{1}{\gamma-1}}, \quad (22)$$

and

$$p_0^*(r^*) = (c_0^{*2})^{\frac{\gamma}{\gamma-1}}, \quad (23)$$

where the radius is non-dimensionalized by the outer radius ( $r^* = r/r_{out}$ ).

For a free vortex swirl, the azimuthal velocity, the mean sound speed, mean density and mean pressure profiles are given by

$$u_{0\phi}^* = \frac{\Gamma^*}{r^*}, \quad (24)$$

$$c_0^{*2}(r^*) = 1 - \left(\frac{\gamma-1}{2}\right)(\Gamma^*)^2 \left(\frac{1}{(r^*)^2} - 1\right), \quad (25)$$

$$\rho_0^*(r^*) = \left[1 - \left(\frac{\gamma-1}{2}\right)(\Gamma^*)^2 \left(\frac{1}{(r^*)^2} - 1\right)\right]^{\frac{1}{\gamma-1}}, \quad (26)$$

and

$$p_0^*(r^*) = \left[1 - \left(\frac{\gamma-1}{2}\right)(\Gamma^*)^2 \left(\frac{1}{(r^*)^2} - 1\right)\right]^{\frac{2}{\gamma-1}}. \quad (27)$$

where  $\Gamma^* = \Gamma/r_{out} c_{0out}$ .

For a rigid body swirl, the azimuthal velocity, the mean sound speed, mean density and mean pressure profiles are given by

$$u_{0\phi}^* = \Omega^* r^*, \quad (28)$$

$$c_0^{*2}(r^*) = 1 - \left(\frac{\gamma-1}{2}\right)(\Omega^*)^2 (1 - (r^*)^2), \quad (29)$$

$$\rho_0^*(r^*) = \left[1 - \left(\frac{\gamma-1}{2}\right)(\Omega^*)^2 (1 - (r^*)^2)\right]^{\frac{1}{\gamma-1}}, \quad (30)$$

and

$$p_0^*(r^*) = \left[1 - \left(\frac{\gamma-1}{2}\right)(\Omega^*)^2 (1 - (r^*)^2)\right]^{\frac{\gamma}{\gamma-1}}, \quad (31)$$

where  $\Omega^* = \frac{\Omega r_{out}}{c_0(r_{out})}$ .

For a combination of free vortex swirl and solid body rotation , the azimuthal velocity, the mean sound speed, mean density and mean pressure profiles are given by

$$u_{0\phi}^* = \frac{\Gamma^*}{r^*} + \Omega^* r^*, \quad (32)$$

$$c_0^{*2}(r^*) = 1 - \left(\frac{\gamma-1}{2}\right) \left[ (\Omega^*)^2 (1 - r^*) + (\Gamma^*)^2 \left(\frac{1}{(r^*)^2} - 1\right) \right] + 2(\gamma-1)\Gamma^*\Omega^*\log r^*, \quad (33)$$

$$\rho_0^*(r^*) = \left\{ \left[ (\Omega^*)^2 (1 - r^*) + (\Gamma^*)^2 \left(\frac{1}{(r^*)^2} - 1\right) \right] + 2(\gamma-1)\Gamma^*\Omega^*\log r^* \right\}^{\frac{1}{\gamma-1}}, \quad (34)$$

and

$$p_0^*(r^*) = \left\{ \left[ (\Omega^*)^2 (1 - r^*) + (\Gamma^*)^2 \left(\frac{1}{(r^*)^2} - 1\right) \right] + 2(\gamma-1)\Gamma^*\Omega^*\log r^* \right\}^{\frac{2}{\gamma-1}}. \quad (35)$$

where  $\Gamma^* = \Gamma/r_{out} c_{0out}$ .

Besides the mean flow axial profile, an axial profile proposed by Posson & Peake<sup>21</sup> was also used. This profile is described as:

$$u_{x0}^{*2}(r^*) = 1 + 2[(\Omega^*)^2 (1 - (r^*)^2) - 2\Omega^*\Gamma^*\ln(r^*)] \quad (36)$$

## II.C. Unsteady Flow

The linearised Euler Equations for a homentropic perturbation field are given by

$$\frac{\partial \rho'}{\partial t} + \nabla \cdot (\rho_0 \mathbf{u}' + \rho' \mathbf{u}_0) = 0, \quad (37)$$

$$\rho_0 \left[ \frac{\partial \mathbf{u}'}{\partial t} + \mathbf{u}_0 \cdot \nabla \mathbf{u}' + \mathbf{u}' \cdot \nabla \mathbf{u}_0 \right] + \rho' [\mathbf{u}_0 \cdot \nabla \mathbf{u}_0] + \nabla p' = 0, \quad (38)$$

and

$$\frac{\partial p'}{\partial t} + \mathbf{u}_0 \cdot \nabla p' + \mathbf{u}' \cdot \nabla p_0 + \gamma p_0 \nabla \cdot \mathbf{u}' + \gamma p' \nabla \cdot \mathbf{u}_0 = 0. \quad (39)$$

Writing Equations (30) to (37) in cylindrical coordinates and assuming the velocity fluctuations to be of the form

$$\mathbf{u}' = u'_r \mathbf{e}_r + u'_\phi \mathbf{e}_\phi + u'_x \mathbf{e}_x, \quad (40)$$

the governing equations for the perturbation field are written as

$$\frac{\partial p'}{\partial t} + \frac{u_{0\phi}(r)}{r} \frac{\partial p'}{\partial \phi} + u_{0x} \frac{\partial p'}{\partial x} + u'_r \frac{\rho_0 u_{0\phi}}{r} + \gamma p_0 \left[ \frac{\partial u'_r}{\partial r} + \frac{1}{r} \frac{\partial u'_\phi}{\partial \phi} + \frac{\partial u'_x}{\partial x} + \frac{u'_r}{r} \right] = 0 \quad (41)$$

$$\frac{\partial u'_r}{\partial t} + \frac{u_{0\phi}(r)}{r} \frac{\partial u'_r}{\partial \phi} + u_{0x}(r) \frac{\partial u'_r}{\partial x} - 2 \frac{u_{0\phi} u'_\phi}{r} + \frac{p'}{\rho_0 c_0^2} \left( -\frac{u_{0\phi}^2}{r} \right) + \frac{1}{\rho_0} \frac{\partial p'}{\partial r} = 0 \quad (42)$$

$$\frac{\partial u'_x}{\partial t} + \frac{u_{0\phi}(r)}{r} \frac{\partial u'_x}{\partial \phi} + u_{0x}(r) \frac{\partial u'_x}{\partial x} + \left( u'_r \frac{\partial u_{0x}(r)}{\partial r} \right) + \frac{1}{\rho_0} \frac{\partial p'}{\partial x} = 0 \quad (43)$$

$$\frac{\partial u'_\phi}{\partial t} + \frac{u_{0\phi}(r)}{r} \frac{\partial u'_\phi}{\partial \phi} + u_{0x}(r) \frac{\partial u'_\phi}{\partial x} + \frac{u_{0\phi} u'_r}{r} + u'_r \frac{\partial u_{0\phi}(r)}{\partial r} + \frac{1}{\rho_0 r} \frac{\partial p'}{\partial \phi} = 0 \quad (44)$$

## II.D. Boundary Condition

For lined ducts the the velocity radial component at the walls is given by the Ingard-Myers Boundary Condition:<sup>12</sup>

$$u_r = n \left( i\omega + \frac{u_{0\phi}}{r} \frac{\partial}{\partial \phi} + u_{0x} \frac{\partial}{\partial x} \right) \frac{p}{i\omega z}, \quad (45)$$

where  $n = +1$  at the outer radius and  $n = -1$  at the hub. For hard-walled ducts, the impedance goes to infinity and Equation (43) reduces to

$$u_r = 0. \quad (46)$$

## II.E. Normal Mode Analysis

Perturbation variables  $\rho', p', u'_r, u'_\phi$  and  $u'_x$  are assumed to have the exponential dependence:

$$f'(r, \phi, x, t) = f(r) e^{i(-k\lambda x + \omega t - m\phi)}, \quad (47)$$

where  $f'$  is the perturbation variable,  $k\lambda = k_x = \omega/c_p$  is the acoustic wavenumber,  $c_p$  is the mode phase speed,  $m$  is the circumferential mode order and  $\omega$  is the frequency. Substituting equation (48) in equations (41) to (44), considering that the mean density does not change with the axial and azimuthal direction, writting the axial wavenumbers on

the right hand side and writing the mean flow velocities in terms of Mach numbers, the governing equations for the perturbation field are written as

$$\left( i\omega - c_0 \frac{M_{0\phi} im}{r} \right) p + c_0^2 \left( \frac{\rho_0 M_{0\phi}^2}{r} + \gamma p_o \left( \frac{\partial}{\partial r} + \frac{1}{r} \right) \right) u_r - \left( \gamma \frac{p_0 mi}{r} \right) u_\phi = -ik\lambda (-c_0 M_{0x} p - \gamma p_0 u_x), \quad (48)$$

$$\left( \frac{1}{\rho_0} \frac{\partial}{\partial r} - \frac{1}{\rho_0} \frac{M_{0\phi}^2}{r} \right) p + \left( i\omega - c_0 \frac{M_{0\phi} im}{r} \right) u_r + \left( -2c_0 \frac{M_{0\phi}}{r} \right) u_\phi = -ik\lambda (-c_0 M_{0x} u_r). \quad (49)$$

$$\left( c_0 \frac{\partial M_{0x}}{\partial r} \right) u_r + \left( i\omega - c_0 \frac{im M_{0\phi}}{r} \right) u_x = -ik\lambda \left( -\frac{p}{\rho_0} - c_0 M_{0x} u_x \right), \quad (50)$$

and

$$-\left( \frac{im}{\rho_0 r} \right) p + \left( c_0 \frac{M_{0\phi}}{r} + c_0 \frac{\partial M_{0\phi}}{\partial r} \right) u_r + \left( i\omega - c_0 \frac{im M_{0\phi}}{r} \right) u_\phi = -ik\lambda (-c_0 M_{0x} u_\phi), \quad (51)$$

where  $M_{0\phi}$  and  $M_{0x}$  are the local Mach numbers in the circumferential and axial directions defined by  $M_{0\phi} = u_{0\phi}/c_0$  and  $M_{0x} = u_{0x}/c_0$  and  $k_x = k\lambda$  is the axial wavenumber. The boundary condition is written as:

$$u_r = n \left( i\omega - im \frac{u_{0\phi}}{r} - ik\lambda u_{0x} \right) \frac{p}{i\omega z}, \quad (52)$$

where  $n = +1$  at the outer radius and  $n = -1$  at the hub. For hard-walled ducts, the boundary condition is reduced to:

$$u_r = 0. \quad (53)$$

### III. Numerical Method

Equations (48) to (51) are written as:

$$[\mathbf{M}]\mathbf{x} = -ik\lambda [\mathbf{N}]\mathbf{x}, \quad (54)$$

where the vector  $\mathbf{x}$  and the matrix operators  $\mathbf{M}$  and  $\mathbf{N}$  are given by:

$$[\mathbf{M}] = \begin{vmatrix} i\omega - c_0 \frac{M_{0\phi} im}{r} & c_0^2 \left( \frac{\rho_0 M_{0\phi}^2}{r} + \gamma p_o \left( \frac{\partial}{\partial r} + \frac{1}{r} \right) \right) & -\gamma \frac{p_0 mi}{r} & 0 \\ \frac{1}{\rho_0} \frac{\partial}{\partial r} - \frac{1}{\rho_0} \frac{M_{0\phi}^2}{r} & i\omega - c_0 \frac{M_{0\phi} im}{r} & -2c_0 \frac{M_{0\phi}}{r} & 0 \\ -\frac{im}{\rho_0 r} & c_0 \frac{M_{0\phi}}{r} + c_0 \frac{\partial M_{0\phi}}{\partial r} & i\omega - c_0 \frac{im M_{0\phi}}{r} & 0 \\ 0 & c_0 \frac{\partial M_{0x}}{\partial r} & 0 & i\omega - c_0 \frac{im M_{0\phi}}{r} \end{vmatrix}$$

$$[\mathbf{N}] = \begin{vmatrix} -c_0 M_{0x} & 0 & 0 & -\gamma p_0 \\ 0 & -c_0 M_{0x} & 0 & 0 \\ 0 & 0 & -c_0 M_{0x} & 0 \\ -\frac{1}{\rho_0} & 0 & 0 & -c_0 M_{0x} \end{vmatrix}$$

and

$$\mathbf{x} = \begin{bmatrix} p \\ u_r \\ u_\phi \\ u_x \end{bmatrix}, \quad (55)$$

In the inner and outer walls, the second line of matrix operators  $\mathbf{M}$  and  $\mathbf{N}$  are substituted by the boundary condition given by Equation (52):

$$u_r = n \left( i\omega - im \frac{u_{0\phi}}{r} - ik\lambda u_{0x} \right) \frac{p}{i\omega z}, \quad (56)$$

where  $n = +1$  at the outer radius and  $n = -1$  at the hub. For hard-walled ducts,  $u_r = 0$  is substituted in matrices  $\mathbf{M}$  and  $\mathbf{N}$  for inner and outer walls.

The eigenvalue problem is discretized using a central fourth-order Finite Difference Method to approximate radial derivatives. In the inner and outer radii, forward and backward schemes were used. The grid is uniform and the derivative matrix is given by:<sup>17</sup>

$$D = \left[ \frac{1}{12\Delta r} \right] \begin{bmatrix} -25 & +48 & -36 & +16 & -3 & . & . & . & . \\ -3 & -10 & +18 & -6 & +1 & . & . & . & . \\ +1 & -8 & 0 & +8 & -1 & . & . & . & . \\ . & . & . & . & . & . & . & . & . \\ & & +1 & -8 & 0 & +8 & -1 & . & . \\ & & & . & . & . & . & . & . \\ & & & & +1 & -8 & 0 & +8 & -1 \\ & & & & -1 & +6 & -18 & +10 & +3 \\ & & & & +3 & -16 & +36 & -48 & +25 \end{bmatrix}, \quad (57)$$

To solve the problem numerically, Equation (54) is written as

$$(-i[\mathbf{N}])\mathbf{x} = c_p \left( \frac{1}{\omega} [\mathbf{M}] \right) \mathbf{x}, \quad (58)$$

where  $c_p$  is the mode phase speed. The eigenvectors and eigenvalues are calculated using the linear algebra library LAPACK, that uses the QZ algorithm.<sup>17</sup> The axial wavenumbers  $k_x = k\lambda$  are calculated by:

$$k_x = \frac{\omega}{c_p} \quad (59)$$

A subset of the modes obtained is not well resolved and should be filtered. Those modes are purely numerical and dominated by point-to-point oscillations. A selective filter developed by Tam<sup>24</sup> retains only shorter wavelength components and uses a 15-point stencil DRP scheme to separate physical modes from numerical ones. The filtered solution is calculated as

$$\tilde{q}(r_n) = \sum_{i=-7}^{+7} a_i q(r_{n+i}) \quad (60)$$

where  $a_i$  are the filter coefficients and  $q$  is the eigenvector. If the mode is well resolved, the filtered eigenvalue  $\tilde{q}$  is much smaller than  $q$ . Otherwise, if the mode is dominated by point-to-point oscillations  $\tilde{q}$  will be of the similar order of  $q(r)$ . The filtered results are compared with the original results as:

$$\alpha = \frac{\| \tilde{q}(r) \|}{\| q(r) \|}, \quad (61)$$

where the norms above are given by:

$$\| f \|^2 = \frac{1}{2} \sum_{n=1}^{N-1} (r_{n+1} - r_n) [r_n f(r_n)^2 + r_{n+1} f(r_n+1)^2] \quad (62)$$

Filtered modes are organized as  $\alpha$  increases and only a subset of those modes are considered.

## IV. Experimental Setup

### IV.A. Configurable Fan Artificial Noise Source

The Configurable Fan Artificial Noise System (CFANS) is based on the Advanced Noise Control Fan presented in figure 1. The ANCF is a highly configurable 4-foot diameter ducted fan located in the Aero-Acoustic Propulsion Laboratory<sup>31</sup> (AAPL) at the NASA Glenn Research Center. The AAPL is a hemispherical anechoic (above 125 Hz.) test facility used for aero-acoustic research. An exterior view of the 65-foot high dome is shown in figure 2. The CFANS can be operated with the fan running (to provide duct flow) or with the fan at 0 rpm, or even removed (to provide a no-flow environment).



Figure 1: The Advanced Noise Control Fan



Figure 2: Aero-Acoustic Propulsion Laboratory

CFANS is utilized to generate and control circumferential modes ( $m$ ) in the audible regime. The system consists of 4 axially distributed rows, each with 16 circumferentially distributed sets of electromagnetic drivers flush mounted on the inner wall. There are two spool pieces, each having 2 driver rows. A Labview<sup>TM</sup> program is used to generate the waveforms sent to each driver independently, in the proper phase relationship to generate the desired circumferential mode. The signals to each row can be adjusted relative to one another to effect the radial distribution, if desired. The practical limits of the system are  $|m - \text{order}| < 7$ , and frequency  $< 1500\text{Hz}$ . A schematic is presented in figure 3. A photograph of the installation for this test program is presented in figure 4.

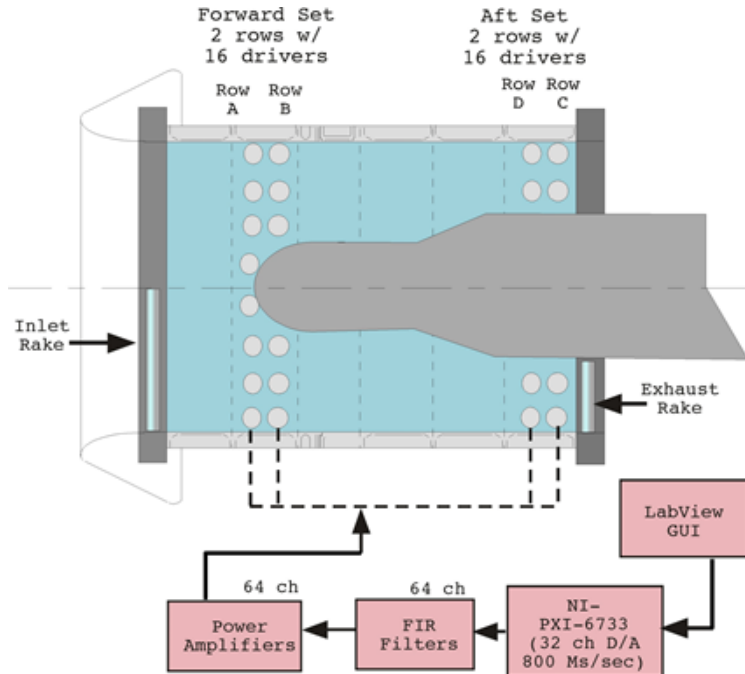


Figure 3: Schematic of the Configurable Fan Artificial Noise System (CFANS)

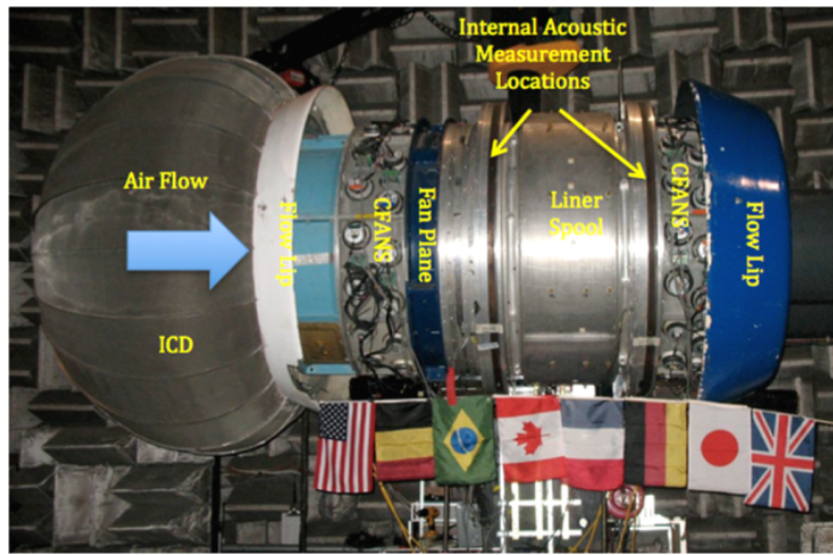


Figure 4: External view of ANCF Showing Relevant Locations

#### IV.B. Assembly of Liner for the Advanced Noise Control Fan

The honeycomb liner core was manufactured separately and incorporated into an existing spool piece. Starting from the outer radius working inward, the liner assembly was as follows: First, 2 layers of carpet padding were laid in the spool in order to provide a compression mechanism for the entire assembly. This mitigated the geometric imperfections of the spool wall, ultimately allowing for a tight fit. Next, a hard rubber sheet was laid down. This provided a seal at the base of the honeycomb core to prevent acoustic leakage between the cells. On top of this was placed the honeycomb core. A fine wire resistance mesh (nominal flow resistance of 60 cgs Rayls) was placed on top of the core, followed by a coarse screen covering approximately 37 percent of the open area. The screen was fastened to the facing of the inner ledge of the spool frame in such a manner to compress the entire lay-up securely and provide a flush flow surface in the duct. The liner depth is 0.0508 m (2.0 in) and the liner length is 0.381 m (16 in). Figure 5 shows the build up of liner side view, while the top view is shown in figure 6 shows the build-up of liner top view.

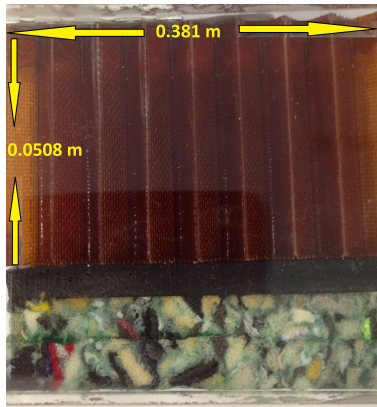


Figure 5: Side view of Liner build up



Figure 6: Top view of liner build-up

The normalized impedance of a 2x2 coupon sample of the liner assembly as measured in the NASA Langley Normal Impedance Tube (NIT)<sup>34</sup> is shown in figure 7.

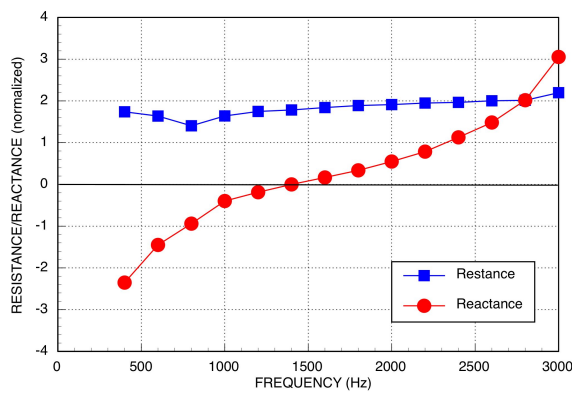


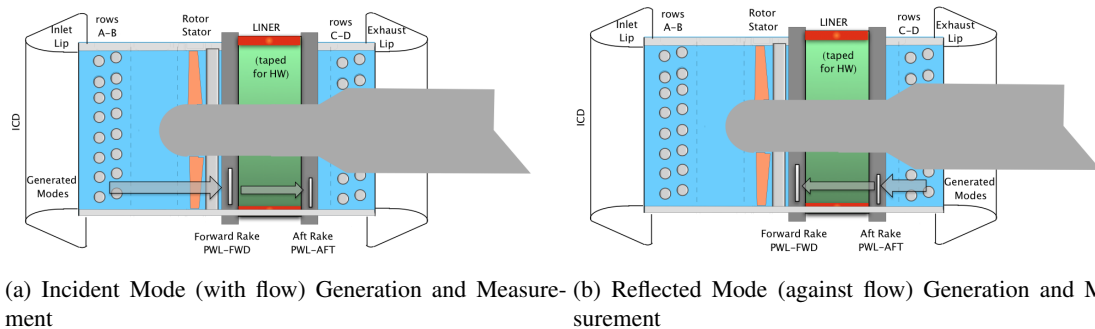
Figure 7: Liner Assembly Impedance Measured in LaRC NIT

#### IV.C. Configurations Tested

The experimental portion of this project test goal was to experimentally measure the liner insertion loss in swirl, no-swirl flow conditions, in the flow direction (incident modes), and against the flow (reflected modes). Swirl is considered to be removed by the presence of the stator vanes, and is considered to remain when the fan is run without the stator vanes installed (rotor alone).<sup>33</sup> Also, the cases were repeated with the fan at idle to represent the no-flow case. These configurations are intended to isolate the effect of geometry change and blockage. The power is measured at the aft and forward rotating rakes.

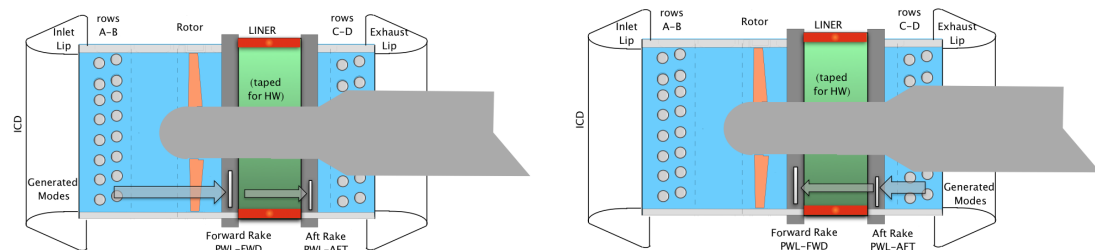
Figures 8 and 9 show schematics of the experimental setups. Axial flow (no-swirl) is achieved when the rotor and the stator are both installed, as shown in figure 8. Modes propagating with the flow (incident modes) are generated by actuator rows A + B and measured by rotating rakes placed immediately upstream of the liner and immediately downstream of the liner. Modes propagating against the flow (reflected modes) are generated by actuator row C; modes are also measured at the two rake locations. A single circumferential mode is generated at a time. Each of these cases was tested with the liner installed, and with the liner taped over to represent the hard-wall case. The transmission loss is measured by the difference in the power measured by those two rakes (in the direction of acoustic propagation) for the lined test minus the transmission loss measured by the difference in the power measured by those two rakes for the hard-walled test, that is:

$$TL = |[(PWL_{FWD,Lined}) - (PWL_{AFT,Lined})] - [(PWL_{FWD,Hard}) - (PWL_{AFT,Hard})]| \quad (63)$$



(a) Incident Mode (with flow) Generation and Measurement (b) Reflected Mode (against flow) Generation and Measurement

Figure 8: Rotor-Stator Installed for No-Swirl Condition



(a) Incident Mode (with flow) Generation and Measurement (b) Reflected Mode (against flow) Generation and Measurement

Figure 9: Rotor-Alone Installed for Swirl Condition

Table I provides the modes generated and the cut-off ratios at relevant duct locations. Note that at the lower m-orders, the n=1 radial can cut-off as it propagates down the duct. This can have significant effect on the modes measured between the two rake stations due to reflections resulting from a mode cutting off.

**TABLE I: Typical Modes Generated for Parametric Studies using CFANS**

FREQ (Hz)	MODES (m;n)	CUT-OFF	RATIOS	( $\sigma$ )	hub-to-tip ratio)
		INLET ( $\sigma=0.0$ ) M# = -0.115	R/S ( $\sigma=.375$ ) M# = +0.130	EXHAUST ( $\sigma=0.5$ ) M# = +0.150	
500	(0, 0); (0, 1)	Inf; 1.48	Inf; 1.09	Inf; 0.87*	
""	+/- (1, 0); (1, 1)	3.08; 1.06	3.81; 1.03	4.20; 0.89*	
""	+/- (2, 0)	1.85	1.97	2.12	
""	+/- (3, 0)	1.35	1.37	1.44	
""	+/- (4, 0)	1.07	1.08	1.10	

\*cut-off

NOTE: Values are for hard-wall, nominal plug flow, flow in direction of standard fan definitions.

## V. Numerical Results: Code Verification

### V.A. Uniform Axial Flow

This session presents results for an annular duct with flow in the absence of swirl. The current finite difference code was verified against results available in the literature and analytical solutions (when possible) by comparing the axial wavenumbers.

Results from the Finite Difference code were first validated against the analytical theory for sound propagation in a hard-walled uniform mean flow for mode  $m=+2$ , mean flow axial mach number  $M_{x0} = 0.3$ , Helmholtz number  $He = 10$  and hub to tip ratio  $\sigma = 0.25$ . Figure 10 shows a comparison between the axial wavenumbers given by the Finite Difference code and analytic solution. Blue crosses refer to results obtained with the FD swirling code and magenta diamonds refer to the analytical solution.

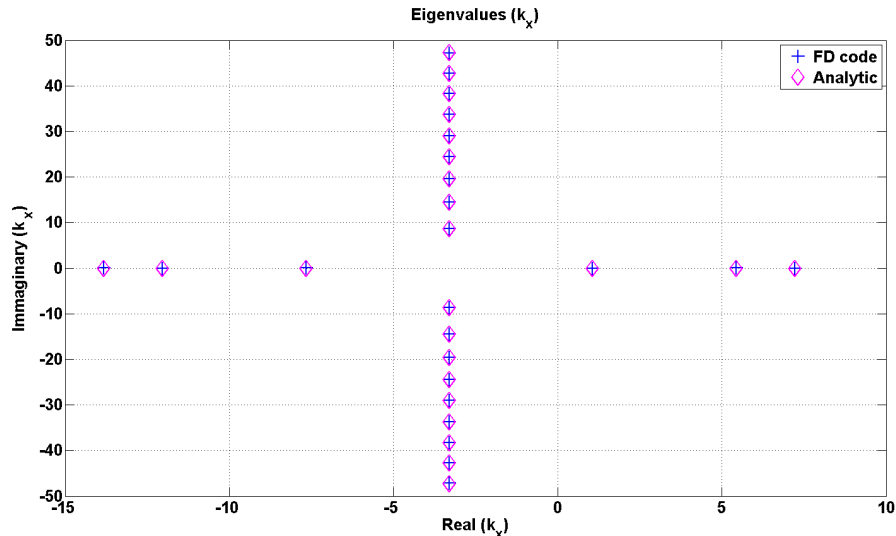


Figure 10: Validation of Swirling Flow code for uniform flow and Hard-walls. Mach=0.3, m=2, He=10

Modes with purely real axial wavenumbers are propagating, cut on, modes. Modes for which the axial wavenumber has an immaginary part are decaying, cut-off modes. If the immaginary part of the axial wavenumber is positive, the mode decays in the negative direction and propagates in the left direction. If the immaginary part of the axial wavenumber is negative, the mode decays in the positive direction and propagates to the right. For the acoustic modes, the cut-off line is given by:

$$\text{Real}(k_x) = \frac{kM_{x0}}{M_{x0}^2 - 1}, \quad (64)$$

that in this case is  $\text{Real}(k_x) = -3.2967$ .

Although only wavenumbers for the acoustic modes are presented in figure 10, there is also a group of hydrodynamic modes that are purely convected by the mean flow and are given by:

$$(k_x)_{\text{convective}} = \frac{k}{M_{x0}}, \quad (65)$$

that in this case are given by  $(k_x)_{\text{convective}} = 33.3$ .

For the case of sound propagation in lined annular ducts with uniform mean flow, results from the finite difference code were compared with results from a shooting method code provided by Dr. Alan McAlpine. Both walls are lined. Figure (11) shows comparison between axial wavenumbers obtained with the current finite difference code and the shooting method code for the sound propagation in an uniform axial flow inside a lined annular duct for mode  $m=+2$ , mean flow axial mach number ( $M_{x0}$ ) 0.3, Helmholtz number  $He = 10$ , hub to tip ratio  $\sigma = 0.25$  and impedance  $1/(2-i)$ . Blue crosses refer to results obtained with the FD swirling code and magenta diamonds refer to the analytical solution.

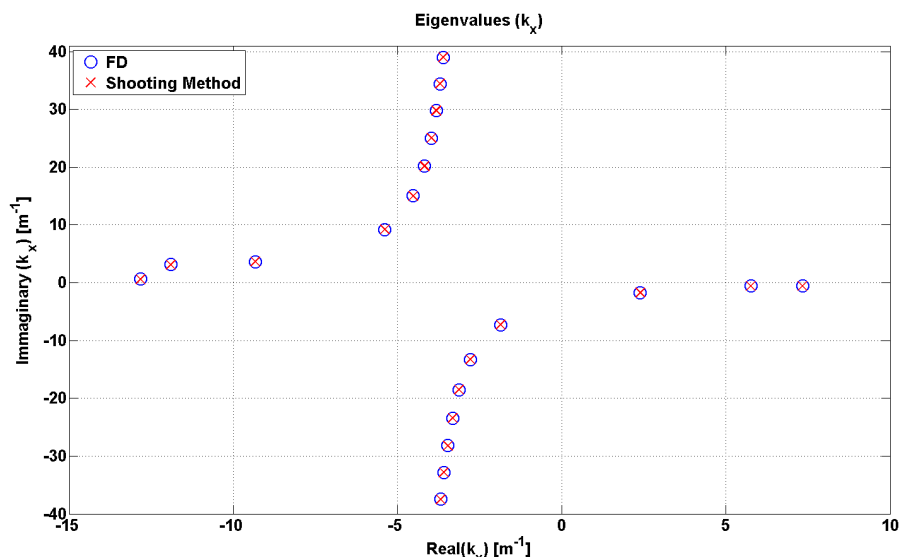


Figure 11: Validation of eigenmode calculation for uniform axial flow and lined walls. Mach=0.3, m=2, He=10,  $z=1/(2-i)$

To the scale shown, the axial wavenumbers obtained with the current finite difference code and with the results available (analytic solution for the hard-walled duct solutions and shooting method code for the lined duct solutions) are indistinguishable.

## V.B. Swirling Flow: Vortex Swirl

The first swirling flow profile to be evaluated is a vortex swirl with a uniform axial mean flow, as studied by Kousen<sup>16</sup> and Nijboer.<sup>18</sup> The parameters used here are mode order  $m = +2$ , axial Mach number  $M_x = 0.3$ , Helmholtz number  $He = 10$ , hub to tip ratio  $\sigma = 0.4$ , magnitude of free vortex swirl  $\Gamma^* = 0.2$  and  $\gamma = 1.4$ . The duct is hard-walled and the reduced frequency is calculated using the sound speed on the outer radius. The mean flow Mach number profile is shown in figure 12

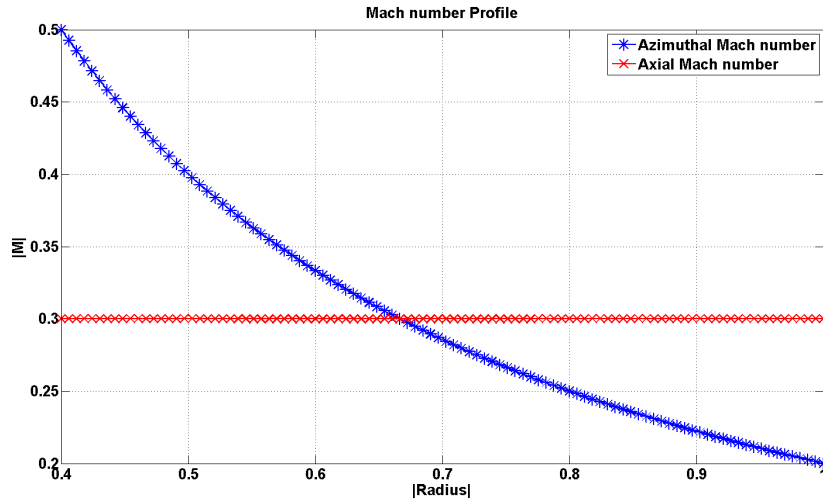


Figure 12: Mean Mach number profile for the vortex swirl case

Figure 13 shows the comparison between axial wavenumbers obtained with the current method and results from Nijboer.<sup>18</sup> The acoustic wavenumbers have real parts between  $-15$  and  $10$  and are distributed symmetrically around the cut-off line at approximately  $Re(k_x) = -3$ . In addition to those acoustic modes, a continuum of modes correspondent to wavenumbers with real part between  $25$  and  $32$  is also found.

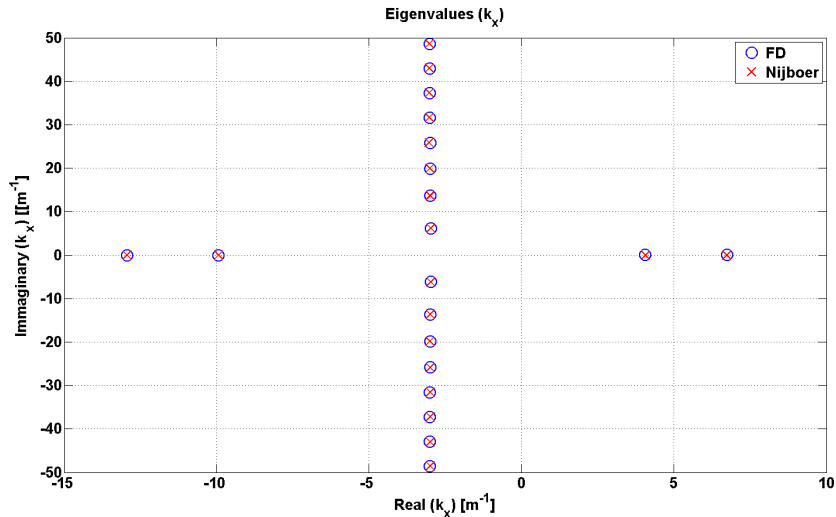


Figure 13: Comparison between results from the finite difference code and results from Nijboer<sup>18</sup> for a vortex swirl mean flow profile and hard-walled duct. Mode order  $m = +2$ , axial Mach number  $M_x = 0.3$ , reduced frequency  $k = 10$ , hub to tip ratio  $\sigma = 0.4$  magnitude of free vortex swirl  $\Gamma^* = 0.2$

### V.C. Swirling Flow: Rigid Body rotation

The second swirling flow profile to be evaluated is a combination of uniform axial flow and rigid body rotation. The parameters used are the same ones proposed by Kousen<sup>16</sup> and reported by Nijboer<sup>18</sup> and Guan et al<sup>9</sup>: mode order  $m = +2$ , axial Mach number  $M_x = 0.3$ , reduced frequency  $k = 10$ , hub to tip ratio  $\sigma = 0.4$  magnitude of free vortex swirl  $\Omega^* = 0.5$ , and  $\gamma = 1.4$ . The duct is hard-walled and the reduced frequency is calculated using the reference sound speed on the outer radius. The mean flow Mach number profile is shown in figure 14

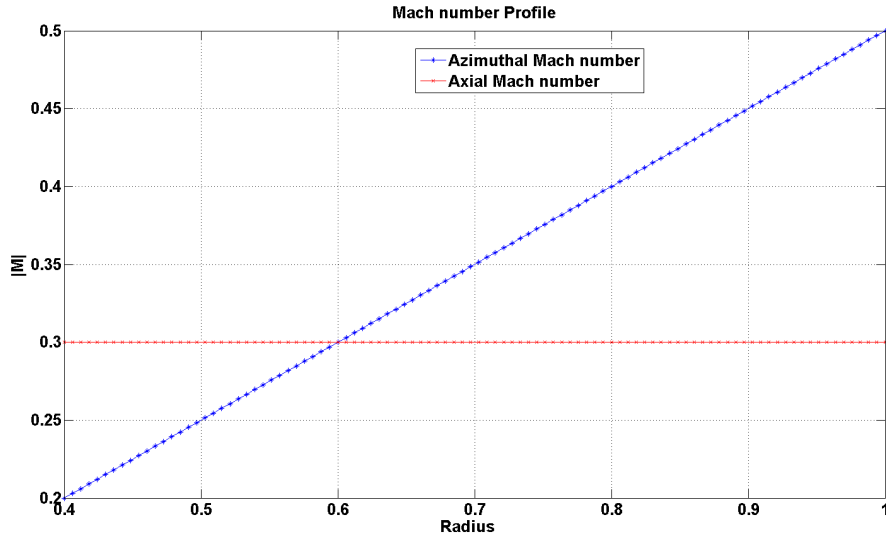


Figure 14: Mean flow Mach number Profile

In figure 15a comparison is shown between results from the current Finite difference code and results from Nijboer.<sup>18</sup> The acoustic wavenumbers have real parts between  $-15$  and  $10$  and are distributed symmetrically around the cut-off line at approximately  $Re(k_x) = -3$ .

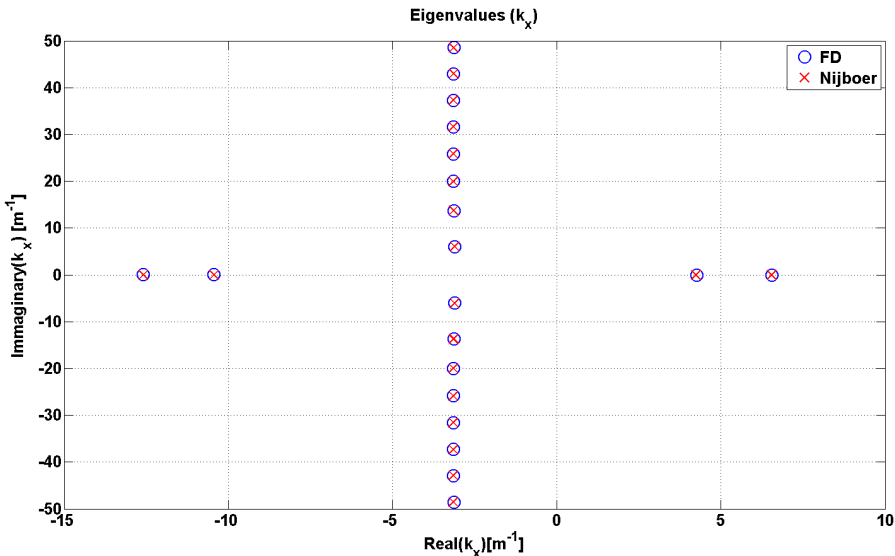


Figure 15: Comparison between results from the finite difference code and results from Nijboer<sup>18</sup> for rigid body swirl and hard-walled duct. Mode order  $m = +2$ , axial Mach number  $M_x = 0.3$ , reduced frequency  $k = 10$ , hub to tip ratio  $\sigma = 0.4$  magnitude of solid body  $\Omega^* = 0.5$

Although not shown in figure 15, a continuum of modes at large values of  $Real(k_x)$  is also found. If the corresponding mode wavenumbers are such as the material derivative of the perturbation is zero, this mode is said to be purely convected. Those nearly convected modes are symmetrically located about the pure convection wavenumber and are nearly unattenuated, which can be seen by the negligible imaginary part of the wavenumber.

#### V.D. Swirling Flow: Rigid Body rotation and Vortex Swirl in a hard-walled duct

The following results were obtained for a swirling mean flow profile which is a combination of rigid body rotation and vortex swirl. The axial velocity profile is the one proposed by Posson & Peake<sup>21</sup> and defined in equation 36. The parameters used here are: mode order  $m = 16$ , reduced frequency  $k = 30$ , hub to tip ratio  $\sigma = 0.5$  magnitude of solid body swirl  $\Omega^* = 0.28$ , magnitude of vortex swirl  $\Gamma^* = 0.1$ , axial Mach number at the tip 0.4 and  $\gamma = 1.4$ . The duct is hard-walled and the reduced frequency is calculated using the sound speed of the outer radius. The mean flow Mach number profile is presented in figure 16

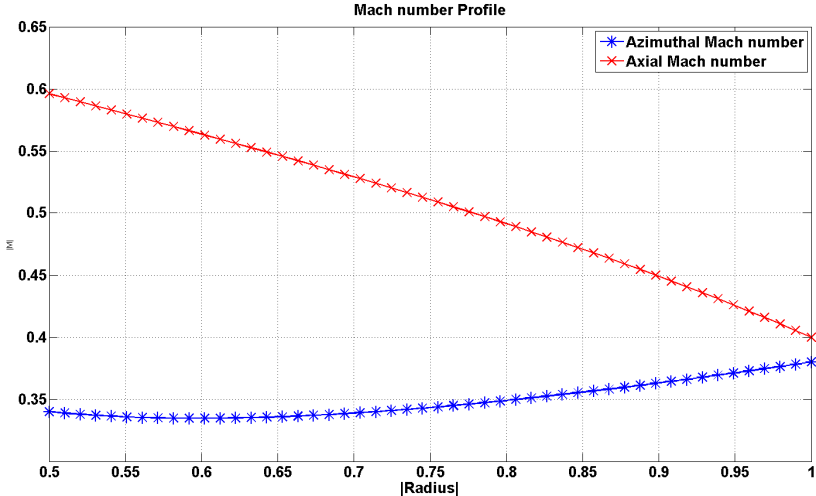


Figure 16: Mean flow Mach number profile: combination of rigid body rotation, vortex swirl and radial equilibrium. Magnitude of solid body swirl  $\Omega^* = 0.28$ , magnitude of vortex swirl  $\Gamma^* = 0.1$  and axial Mach number at the tip 0.4.

Figure 17 shows a comparison between results from the current Finite difference code and results from Posson & Peake.<sup>21</sup> The acoustic wavenumbers have real parts between  $-35$  and  $9$ . A continuum of modes with axial wavenumbers with real parts between  $32$  and  $59.73$  is observed.

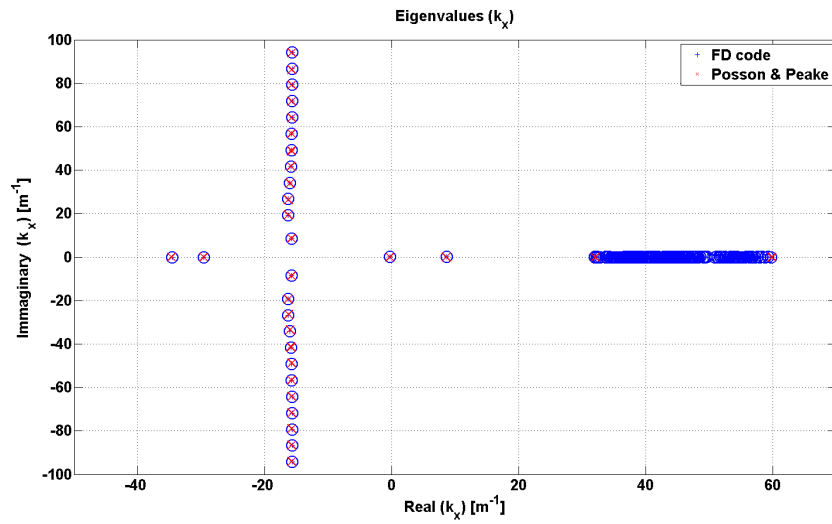


Figure 17: Comparison between results from the current finite difference code and results from Posson & Peake.<sup>21</sup> Mode order  $m = 16$ , reduced frequency  $k = 30$ , hub to tip ratio  $\sigma = 0.5$  magnitude of solid body  $\Omega^* = 0.28$ , magnitude of vortex swirl  $\Gamma^* = 0.1$  and axial Mach number at the tip 0.4.

## V.E. Swirling Flow: Rigid Body rotation and Vortex Swirl in a lined duct

The following results include the effect of a liner with impedance  $z = 1 + 2i$ . As in the previous results, the swirling mean flow profile is a combination of rigid body rotation and vortex swirl. The magnitude of solid body swirl is  $\Omega = 0.28$  and magnitude of vortex swirl  $\Gamma = 0.1$ . The axial profile is the one proposed by Posson & Peake<sup>21</sup> defined in equation 36 and the axial Mach number at the tip is 0.4. The remaining parameters used are: mode order  $m = 16$ , reduced frequency  $k = 30$ , hub to tip ratio  $\sigma = 0.5$  and  $\gamma = 1.4$ . The reduced frequency is calculated using the sound speed of the outer radius. The mean flow Mach number profile is presented in figure 18

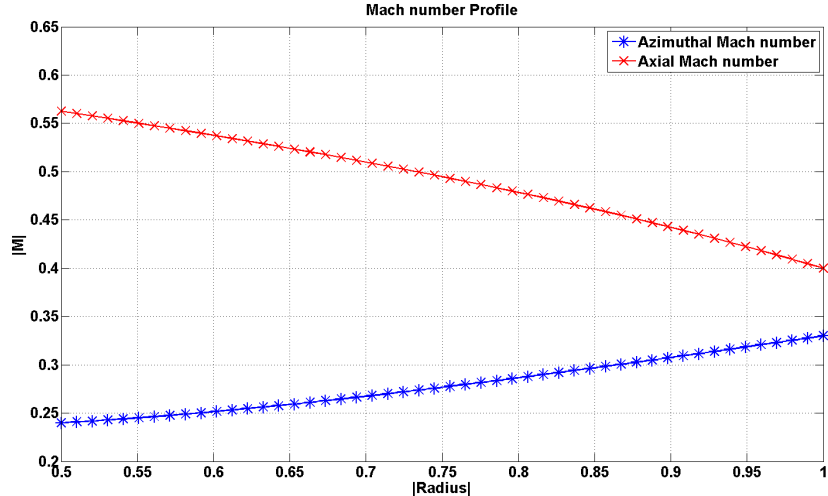


Figure 18: Mean flow Mach number profile for the lined case. Magnitude of solid body swirl  $\Omega^* = 0.28$ , magnitude of vortex swirl  $\Gamma^* = 0.05$  and axial Mach number at the tip 0.4.

Figure 19 shows a comparison between results from the current Finite difference code and those from Posson & Peake.<sup>21</sup> The acoustic wavenumbers have real parts between  $-35$  and  $9$ . A continuum of modes with axial wavenumbers with real parts between  $-39.52$  and  $61.76$  is observed.

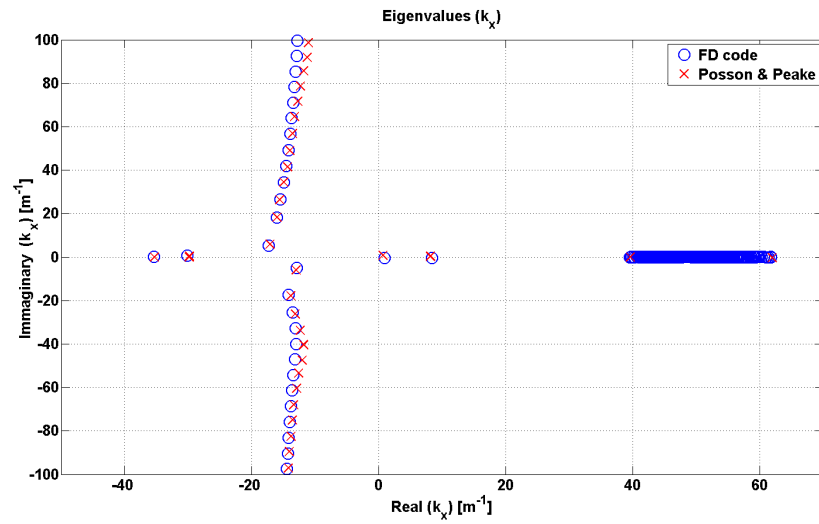


Figure 19: Comparison between results from the current finite difference code and those from Posson & Peake.<sup>21</sup> Mode order  $m = 16$ , reduced frequency  $k = 30$ , hub to tip ratio  $\sigma = 0.5$  magnitude of solid body  $\Omega^* = 0.28$ , magnitude of vortex swirl  $\Gamma^* = 0.05$ , liner impedance  $z = 1 + 2i$  and axial Mach number at the tip 0.4.

## VI. Comparison with Experimental Data

Results from the Finite Difference code were compared to measured data from the Advanced Noise Control Fan for the case of modes propagating upstream (generated by actuator C) and frequency of 500Hz. This subset of results was chosen for comparison because of the absence of blockage effects by the rotor blades and stator vanes. Hot-wire measurements were used to infer the mean flow profile of the axial and swirl velocities. A fit in the hot-wire measurements for the swirl velocity data showed that the azimuthal velocity profile is very similar to a combination of rigid body and vortex swirl swirling flows (given by Eq. 66). The rigid body swirling flow is dominant. The axial profile is close to an uniform axial flow. The mean axial and swirl Mach number profiles are shown in Figure 20 and the swirl Mach number has been represented by:

$$u_{\phi 0} = 44.05r + \frac{0.05234}{r} \quad (66)$$

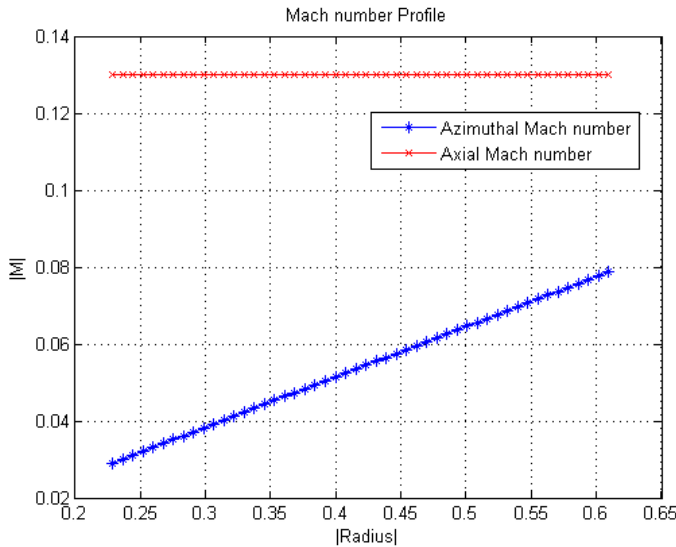


Figure 20: Mean flow

The liner impedance is taken to be  $z = 1.5 - 1.975i$  from the measured data (see Figure 7 above). The transmission loss for the experimental data is calculated using Eq. 63. For the numerical results, the sound power transmission loss for a single mode is calculated as<sup>9</sup>

$$TL = 10\log_{10} \frac{W_{in}}{W_{out}} = 20 \times \text{Imag}(k_x) \times L \times \log_{10} e \quad (67)$$

where  $L$  is the liner length. At this frequency there is only one cut-on radial mode for  $m=0$  in the hardwall section, therefore it is assumed that all the power is contained in the first radial mode of the lined section.

Figure 21 shows the comparison for the no flow case. The transmission loss predicted by the FD code agrees well with the measured data for spinning modes  $|m| \geq 1$ , except for  $m = -4$ . On the other hand the agreement is unsatisfactory for  $m=0$  and  $|m|=1$ , but the reasons for this are not yet understood. Both the FD and ANCF data exhibit a larger TL for negative spinning modes compared to their positive counterpart, with the measured difference being larger than predicted; the agreement between the FD prediction and ANCF data is generally better for the negative spinning modes

The comparison for axial flows is shown in figure 22. Modes  $m = 0$  and  $m = \pm 1$  again show some discrepancy. The FD results are still symmetrical in axial flow, but the experimental data TL shows an increase in the positive modes this may indicate that the stator vanes do not remove all the swirl. Modes  $m = \pm 4$  show a disagreement. Earlier data from the ANCF show mode 4 has significant reflection due to the unique coupling to the duct geometry.

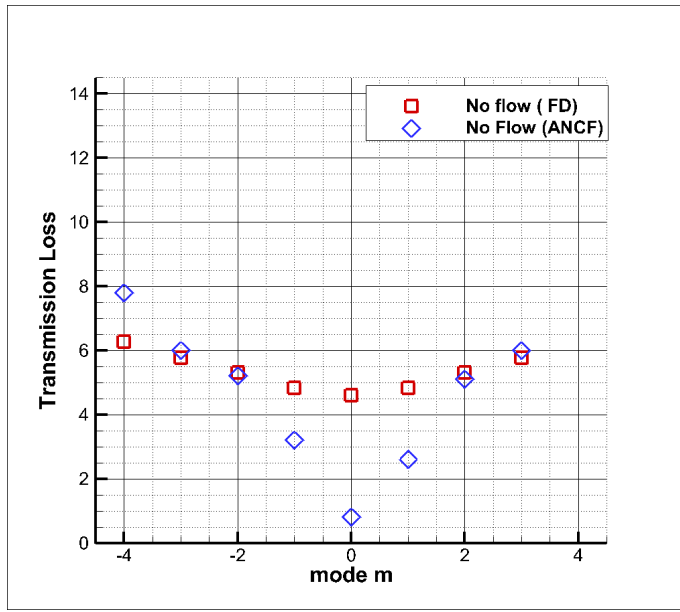


Figure 21: Comparison between predicted results from the current FD code and ANCF data for the no flow case.

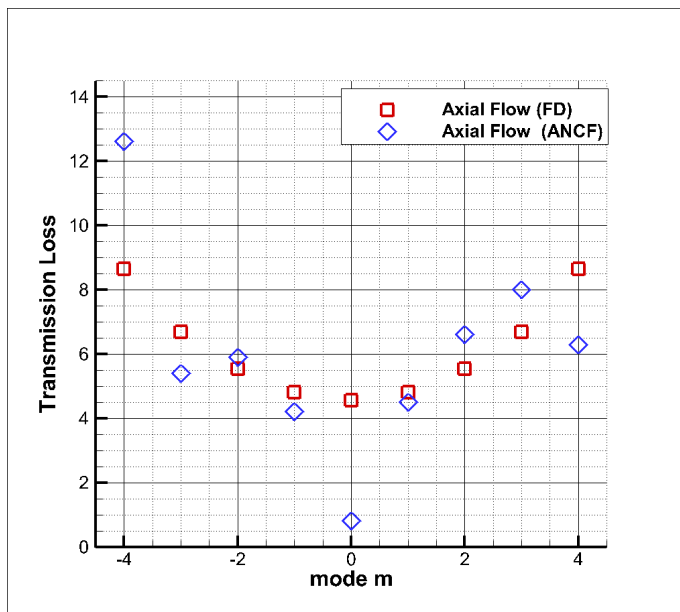


Figure 22: Comparison between predicted results from the current FD code and ANCF data for the case when axial flow is present.

The comparison for swirl flow is shown in figure 23. Both the FD and the ANCF experimental data show an increase in the TL as an effect of the swirl; the agreement between the FD prediction and the ANCF data is better for the negative modes

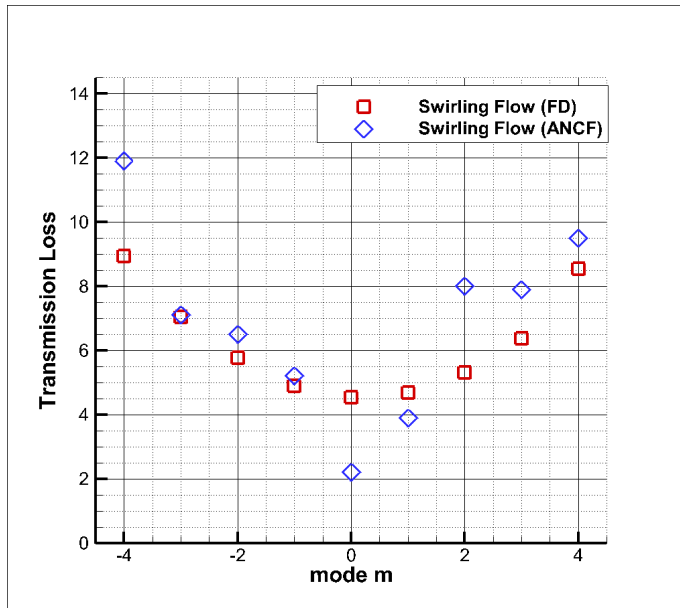


Figure 23: Comparison between predicted results from the current FD code and ANCF data for the swirling flow case.

The FD results for the three flow conditions are shown in Figure 24 and the corresponding measured data in Figure 25. As expected the predicted transmission loss in Figure 24 is symmetric with  $\pm m$ -order; is symmetric with respect to spinning mode number for the no flow and axial flow cases, whereas for the swirling flow case there is a slight asymmetry, as expected. The ANCF measured data in Figure 25 is qualitatively similar but at these modest TL levels, it is difficult to detect any significant trends with flow condition, given that the experimental accuracy is judged to be  $\pm 1$  dB.

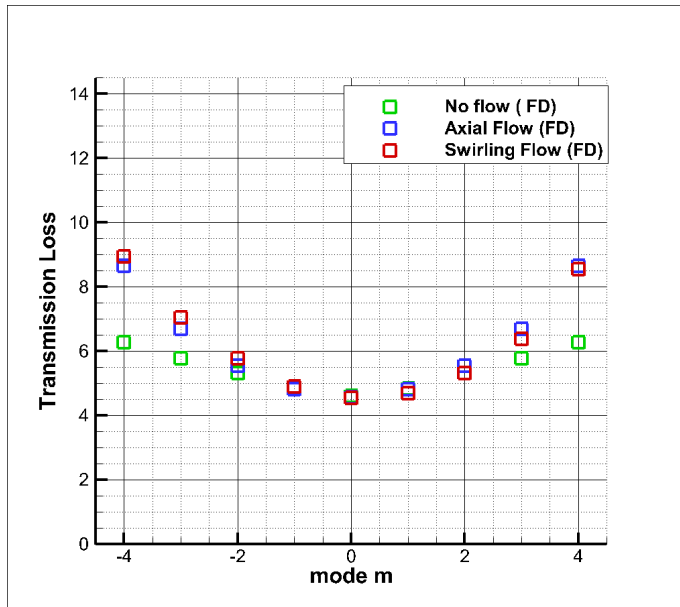


Figure 24: Computed Data

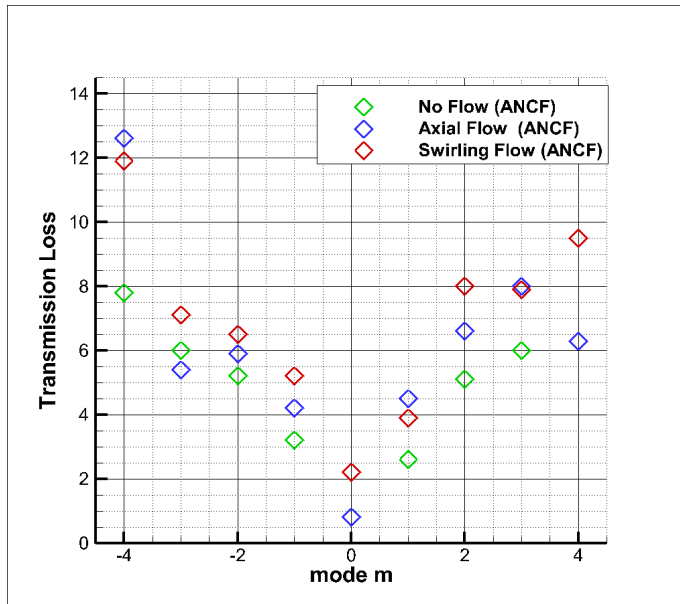


Figure 25: Experimental Data

## VII. Conclusion

A fourth-order finite-difference (FD) code is proposed to evaluate sound propagation in lined annular ducts with swirling flows. The FD code is verified for both uniform axial flow in lined ducts and for swirling flows in annular hard-walled ducts by comparing with available numerical and analytical results and good agreement has been demonstrated in all cases. A preliminary comparison has been conducted of predictions from the FD code with experimental results from the low speed Advanced Noise Control fan at one frequency over a range of spinning mode numbers. Qualitative agreement is obtained with the measured Power Transmission loss (TL) but low Mach numbers and modest TL levels have made it difficult to validate the FD code thus far. As a future work, a parametric analysis of lined ducts with swirling flows is planned.

## Acknowledgments

The first author is the recipient of a Dorothy Hodgkin Postgraduate Award jointly funded by the Engineering and Physical Sciences Research Council (EPSRC) of the UK and Rolls-Royce plc. The remaining authors from the University of Southampton are supported within a more general programme of research by Rolls-Royce University Technology Centre in Gas Turbine Noise at the University of Southampton.

The first author would like to thank Brian Tester for his helpful advice on all aspects of this work, in particular for contributing liner design expertise and for coordinating the work on the liner specification with the second author and fourth authors and Mike Jones at NASA Langley. The first author would also like to thank Paul Murray for fruitful discussions.

The authors would like acknowledge the contributions of Mr. Michael Jones of the NASA Langley Research Center for providing the liner impedance measurements. They would also like to acknowledge the contributions of Hexcel, Inc., for manufacturing the honeycomb core and to the NASA Glenn TFOME crew for their support in model assembly and testing.

## References

- <sup>1</sup>Cooper, A. J. and Peake, N. , *Upstream-radiated rotor-stator interaction noise in mean swirling flow*, Journal of Fluid Mechanics, Vol. 523, 2005, pp. 219-250.
- <sup>2</sup>Cooper, A. J. and Peake, N. , *Propagation of Unsteady Disturbances in Slowly Varying Duct with Mean Swirling Flow*, Journal of Fluid Mechanics, Vol. 445, pp. 207-234, 2001.
- <sup>3</sup>Cooper, A. J. , *Effect of mean entropy on unsteady disturbance propagation in a slowly varying duct with mean swirling flow*, Journal of Sound and Vibration, Vol. 291, pp. 779-801, 2006.
- <sup>4</sup>Golubev, V. V. , Atassi, H. M., *Aerodynamic and acoustic response of a blade row in unsteady swirling flow*, Proceedings of the first joint CEAS/AIAA Aeroacoustics Conference, Munich, Germany, 1995
- <sup>5</sup>Golubev, V. V. , Atassi, H. M., *Acoustic-Vorticity Modes in an Annular Duct with Mean Vortical Swirling Flow*, 3rd AIAA/CEAS Aeroacoustics Conference, Atlanta, GA, 1997, AIAA Paper 97-1695.
- <sup>6</sup>Golubev, V. V. , Atassi, H. M., *Acoustic-vorticity waves in Swirling Flows*, Journal of Sound and Vibration, Vol. 209, 1998, pp. 203-222.
- <sup>7</sup>Golubev, V. V. , Atassi, H. M., *Sound Propagation in an Annular Duct with Mean Potential Swirling Flow*, Journal of Sound and Vibration, Vol. 198, 1996, pp. 601-616.
- <sup>8</sup>Golubev, V. V. , Atassi, H. M., *Unsteady Swirling Flows in annular cascades. Part 1: Evolution of incident disturbances*, AIAA Journal, Vol. 38, pp. 1142-1149, 2000.
- <sup>9</sup>Guan, Y. Luo, K.L. and Wang, T. Q., *Sound Transmission in Lined Annular Duct with Mean Swirling Flow*, NoiseCon 2008/ASME NCAD, Dearborn, Michigan, USA, NCAD2008-73081.
- <sup>10</sup>Guan, Y., Wang, T., *Effect Mean Entropy on Eigenmodes in Annular Duct with Swirling Flow*, 13th AIAA/CEAS Aeroacoustics Conference, Rome, Italy, 2007, AIAA 2007-3536.
- <sup>11</sup>Heaton, C. J. and Peake,N., *Algebraic and exponential instability of inviscid swirling flow*, Journal of Fluid Mechanics, Vol. 565, 2006, pp. 279-318.
- <sup>12</sup>Ingard, U., *Influence of fluid motion past a plane boundary on sound reflection, absorption and transmission*, Journal of Acoustical Society of America, Vol. 31(7), 1959, pp. 1035-1036.
- <sup>13</sup>Kerrebrock, L., *Waves and Wakes in Turbomachine Annuli with Swirl*, AIAA Journal , Vol. 15, pp. 794-803,1974.
- <sup>14</sup>Kerrebrock, L. , *Small Disturbances in Turbomachine Annuli with Swirl*, AIAA Journal, Vol. 15, pp. 794-803, 1977.
- <sup>15</sup>Kousen, K. *Eigenmode Analysis of Ducted Flows with Radially Dependent Axial and Swirl Components.*, AIAA paper 95-160, 1995.
- <sup>16</sup>Kousen, K. *Pressure Modes in Ducted Flows with Swirl.*, AIAA paper 96-1679, 1996.
- <sup>17</sup>Kousen, K. *Eigenmodes of Ducted Flows with Radially-Dependent Axial and Swirl velocity Components.*, NASA CR 1999-208881.
- <sup>18</sup>Nijboer, R., *Eigenvalues and Eigenfunctions of ducted swirling flows*, 7th AIAA/CEAS Aeroacoustics Conference, Maastricht, Netherlands, 2001, AIAA 2001-2178.
- <sup>19</sup>Peake, N. and Parry, A. B. *Modern Challenges Facing Turbomachinery Aeroacoustics*, Annu. Rev. Fluid Mechanics, Vol. 44, pages 227-248, 2012.
- <sup>20</sup>Posson, H. and Peake, N. *The acoustic analogy in an annular duct with swirling mean flow.*, Journal of Fluid Mechanics, Vol. 726, pages 439-475, 2013.
- <sup>21</sup>Posson, H. and Peake, N. *Swirling Mean Flow Effect on Fan-trailing Edge Broadband Noise in a Lined Annular Duct.*, 19th AIAA/CEAS Aeroacoustics Conference, AIAA 2013-2150
- <sup>22</sup>Tam, C. K. and Ariault, L.. *The wave modes in Ducted Swirling Flows*, Journal of Fluid Mechanics, Vol. 371, pages 1-20, 1998.
- <sup>23</sup>Tyler, J. M. and Sofrin, T. G. , *Axial Flow Compressor Noise Studies*, SAE Transactions, Vol. 309, pp. 32, 1965.
- <sup>24</sup>Christopher K. W. Tam , *Computational Aeroacoustics. A wave Number Approach*, Cambridge Aerospace Series. ISBN 978-0-521-80678-7, 2012.
- <sup>25</sup>Myers, M. K. . *An exact energy corollary for homentropic Flow.*, Journal of Sound and Vibration, Vol. 109, pages 277-284, 1986.
- <sup>26</sup>Myers, M. K. . *Generalization and Extension of the Law of Acoustic Energy Conservation in a Non-uniform Flow*, 24th Aerospace Science Meeting, Reno, Nevada, January 6-9, AIAA-86-0471, 1986
- <sup>27</sup>Myers, M. K. . *Transport of Energy by Disturbances in Arbitrary Steady Flows*, Journal of Fluid Mechanics, Vol. 226, pages 383-400, 1991.
- <sup>28</sup>Rienstra, S. W. and Hirshberg, A. , *An Introduction to Acoustics*, Tech Report Eindhoven University of Technology, 2004.
- <sup>29</sup>Atassi, O. V.,*Computing the Sound Power in Non-uniform Flow*, Journal of Sound and Vibration, Vol. 266, 2003, pp. 75-92.
- <sup>30</sup>Morfe, C. L., *Acoustic Energy in Nonuniform Flows*, Journal of Sound and Vibration, Vol. 14,1971, pp. 159-170.
- <sup>31</sup>Loew, R.A., Lauer, J.T., McAllister, J., and Sutliff D.L.,*The Advanced Noise Control Fan*, NASA/TM2006-214368,also AIAA2006-3150.
- <sup>32</sup>B.A. Cooper,*A Large Hemispherical Chamber Enclosure for Community-Compatible Aeroacoustic Testing of Aircraft Propulsion Systems*, Journal of the Institute of Noise Control Engineering of the USA, Jan/Feb 1994.
- <sup>33</sup>McAllister, J., Loew, R.A., Lauer, J.T., and Sutliff, D.L.,*The Advanced Noise Control Fan Baseline Measurements*, NASA/TM2009-215595, also AIAA2009-0624Oct 2009.
- <sup>34</sup>Smith, C.D. and Parrott, T.L.,*Comparison Of Three Methods For Measuring Acoustic Properties Of Bulk Materials*,Journal of Acoustical Society of America, Vol. 74, No. 5, 1983, pp. 1577-1582.